AD-A151 697 HIGH FREQUENCY ESTIMATION OF TWO-DIMENSIONAL CAVITY SCATTERING(U) AIR FORCE INST OF TECH WRIGHT-PATTERSON AFB OH SCHOOL OF ENGINEERING R S DERING DEC 84 1/1

UNCLASSIFIED AFIT/GE/ENG/84D-24 F/G 17/9 NL

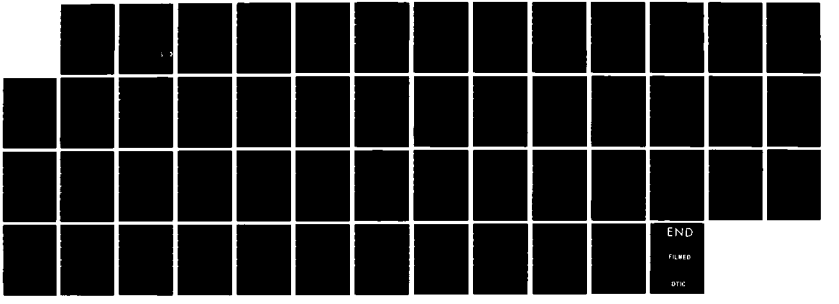

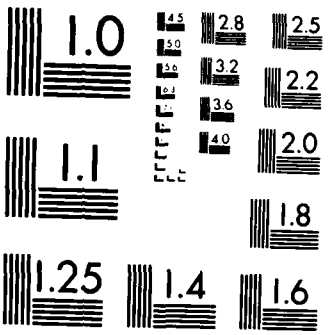

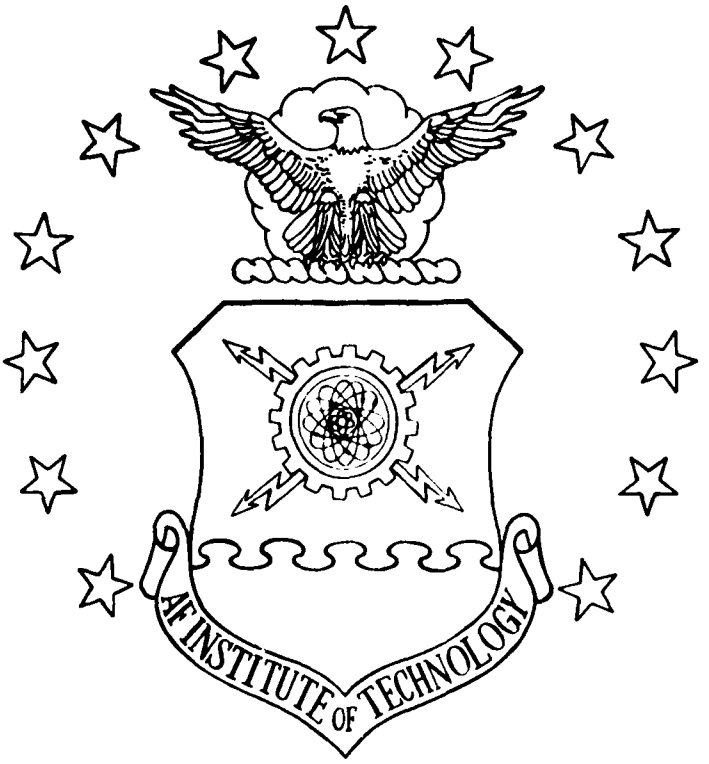

HIGH FREQUENCY ESTIMATION OF TWO-DIMENSIONAL CAVITY SCATTERING

THESIS

Robert Scott Dering
First Lieutenant, USAF

AFIT/GE/ENG/84D-24

DEPARTMENT OF THE AIR FORCE
AIR UNIVERSITY
AIR FORCE INSTITUTE OF TECHNOLOGY

Wright-Patterson Air Force Base, Ohio

AFIT/GE/ENG/84D-24

HIGH FREQUENCY ESTIMATION OF TWO-DIMENSIONAL CAVITY SCATTERING

THESIS

Robert Scott Dering
First Lieutenant, USAF

AFIT/GE/ENG/84D-24

Approved for public release; distribution unlimited

AFIT/GE/~~84D~~ENG/84D-24

HIGH FREQUENCY ESTIMATION OF TWO-DIMENSIONAL CAVITY SCATTERING

THESIS

Presented to the Faculty of the School of Engineering
of the Air Force Institute of Technology
Air University
In Partial Fulfillment of the
Requirements for the Degree of
Master of Science in Electrical Engineering

Robert Scott Dering, B.S.
First Lieutenant, USAF

December 1984

Acknowledgements

I wish to express my appreciation to my faculty advisors Dr. Andrew Terzuoli, Lt. Randy Jost, and Dr. Vital Pyoti for their assistance in this effort. Also, Carl Shortt and John Brohas were very cooperative in the construction of the aluminum cavity. I am also indebted to Lt. John Ward for the generous use of his personal computer. And finally, I am very grateful for Diane Tilley's patience and dedication during the preparation of the final copy of this thesis.

Robert Scott Dering

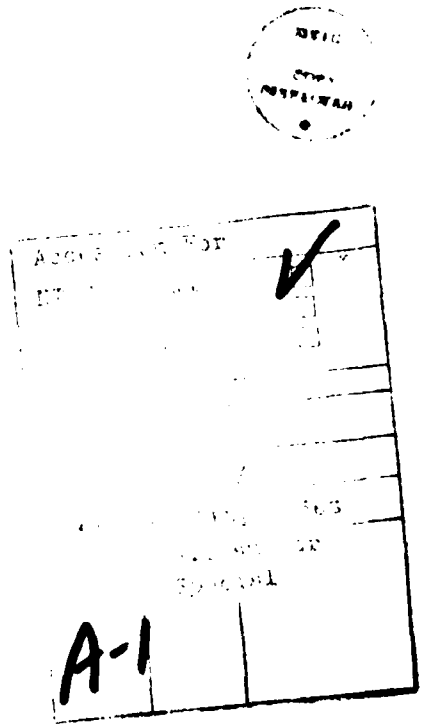

Table of Contents

List of Figures

Abstract

A simple ray tracing approximation for the high frequency scattering from a two-dimensional cavity is developed. Whereas many other cavity scattering algorithms are very time consuming, this method is very swift.

The analytical development of the ray tracing approach is performed in great detail, and it is shown how the radar cross section (RCS) depends on the cavity's length and width, and the radar wave's angle of incidence. This explains why the cavity's RCS oscillates as a function of incident angle. The RCS of a two-dimensional cavity was measured experimentally, and these results were compared to computer calculations based on the high frequency ray tracing theory. The comparison was favorable in the sense that angular RCS minimums and maximums were predicted exactly even though absolute accuracy of the RCS magnitude decreased for incident angles far off-axis. Overall, once the method is extended to three dimensions, this technique shows promise as a fast first approximation of high frequency cavity scattering.

HIGH FREQUENCY ESTIMATION OF TWO-DIMENSIONAL CAVITY SCATTERING

I. Introduction

In recent years, the United States Air Force has devoted much effort to low observables technology. Popularized in the media by the term "stealth," this area of research has created a revolution in electronic warfare strategy. Whereas the survivability of combat aircraft was previously thought to depend on sophisticated jamming equipment, the emphasis has now shifted to the design of aircraft capable of flying undetected through enemy radar coverage. However, the task of reducing an aircraft's radar "echo" is far from trivial. Until recently, this echo, commonly referred to as radar cross section (RCS), could not be accurately predicted; it required actual measurement. This approach is woefully inadequate for the design of modern aircraft because the iterative construction, measurement, and modification of an airframe wastes both time and money. An ideal solution would be a computer program capable of estimating the RCS of any given shape. This would provide the engineer with the additional advantage of being able to try many more approaches to a particular design problem before settling on a final solution.

Unfortunately, no single comprehensive airframe RCS calculation algorithm has been developed because the task of predicting the RCS of even simple structures is staggeringly complex. For now, the building block approach is being used to work toward the eventual completion of a comprehensive RCS calculation project. One of the basic airframe structures which is critical to this process is the engine inlet cavity. It can dominate the aircraft's RCS from several different aspects, and the calculation of its RCS is not trivial for even the simplest cavity designs. Electromagnetic scattering from cavities has been extensively studied. Moll and Seecamp analyzed an inlet modelled by a open-ended cylindrical waveguide. The field entering the cavity's opening is represented by a series of waves traveling inward while the backscattered field is a series of waves moving from the cavity's closed end toward the opening. The sum of these two fields is then equated to the total field at the cavity's opening, and the Stratton-Chu integral is used to solve for the scattered field (4).

Johnson and Moffatt used the Wiener-Hopf technique to find the scattering matrices for the cavity's open end, and the Green's function and Moment Method were employed to find the matrix for the termination of the cavity. The RCS is found after calculating a backscatter coefficient for the entire structure (2).

And finally, Cooper used the method of coupled azimuthal potentials and appropriate Dirichlet boundary conditions to solve for the fields across the cavity's opening (2).

Although these are only several of the studies which analyze the cavity scattering problem, they encompass most of the basic techniques. However, these methods typically suffer from one serious drawback. They all tend to be computationally intensive. A simpler and faster technique could have some applications even if it was not as accurate as any of the methods described above. A simple approach could even be used as a fast first approximation for other more time consuming techniques when great accuracy is required. Furthermore, the majority of the existing cavity scattering methods analyze cylindrically shaped cavities, whereas many inlets of critical concern to RCS engineers have rectangular openings.

The ray tracing method for the analysis of cavity scattering described in this thesis is extremely fast, and it applies primarily to cavities with rectangular openings. It is limited to the high frequency case where the cavity opening is much larger than the wavelength of the incident electromagnetic energy. Also, in an affort to simplify this preliminary attempt at developing ray tracing theory, the analysis is limited to two-dimensional cavities (see Chapter III). Once the success of this technique has been

demonstrated for the two-dimensional case, it should not be difficult to extend it to three dimensions. The ray tracing method calculates RCS as a function of wavelength, cavity width and depth, and incident angle.

II. Analytical Development of the Ray Tracing Approach

Introduction

Before the complex scattering mechanisms present in three-dimensional cavities can be understood, it is both instructive and informative to develop a model to analyze the scattering from a two-dimensional cavity. Although understanding the cross section of a two-dimensional cavity provides no direct benefit since these structures are rarely encountered, the analysis techniques are simple and straightforward. Once an accurate and easily implemented method for predicting the RCS of the simple two-dimensional cavity can be developed, these same techniques can eventually be expanded to treat a three-dimensional case as well. Although a three-dimensional theoretical model is the ultimate goal, an accurate two-dimensional model is a necessary and important step toward achieving that end.

First, a definition of a two-dimensional cavity is in order. As shown in Fig. 2-1, the cavity has two finite dimensions (L and w) but it is infinite in the third dimension (perpendicular to the page). The direction of incident electromagnetic radiation is shown as θ. This angle can vary from -90 to 90 degrees but only within the plane of the page. This restriction will limit the necessary

When the effective length exactly equals three-quarters of a cavity wavelength, all of the incident radar energy is backscattered. This phenomenon is shown in Fig. 2-12.

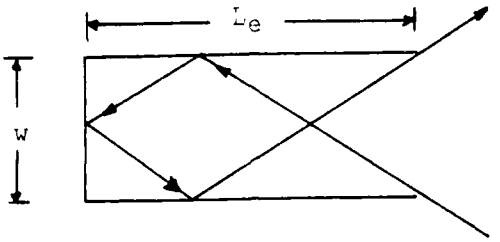

Fig. 2-12. Total Backscatter

All the incident rays enter the cavity above this boundary ray, so all the energy is backscattered.

Case 4

This case occurs when the cavity's effective length is between three-quarters and one full cavity wavelength ($3\lambda/4 < L_e < \lambda$). Fig. 2-14 shows a case 4 cavity with its boundary ray. All incident rays entering below this boundary ray will be backscattered.

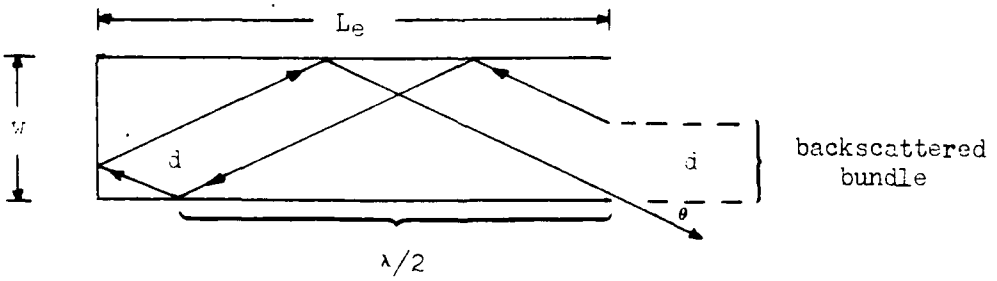

Fig. 2-13. Case 4 Cavity

Case 3

This case occurs when the effective length is between one-half and three-quarters of a cavity wavelength ($\lambda/2 < L_e < 3\lambda/4$).

Fig. 2-11 shows a Case 3 cavity with its boundary ray. The backscatter bundle enters the cavity above this ray, and once again the percentage of the total power that is backscattered is

$$\% \text{ backscatter} = \frac{d}{w}$$

where

$$\tan\theta = \frac{d/2}{L_e - \lambda/2}$$

or

$$d = 2(L_e - \lambda/2)\tan\theta$$

so

$$\% \text{ backscatter} = \frac{d}{w} = \frac{2(L_e - \lambda/2)\tan\theta}{w}$$

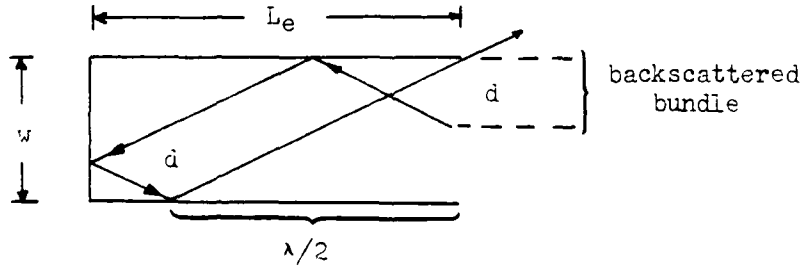

Fig. 2-11. Case 3 Cavity

is reflected in the $-\theta$ direction, and none is backscattered. This is illustrated in Fig. 2-10. Any ray entering above this boundary ray will be reflected, so every ray entering the cavity will exit at an angle of $-\theta$. As previously noted, this instance of total backscatter occurs when

$$L_e = \lambda/2$$

and

$$\tan \theta = \frac{w}{\lambda/2} = \frac{w}{L_e}$$

or

$$\theta = \arctan\left[\frac{w}{\lambda/2}\right] = \arctan\left[\frac{w}{L_e}\right]$$

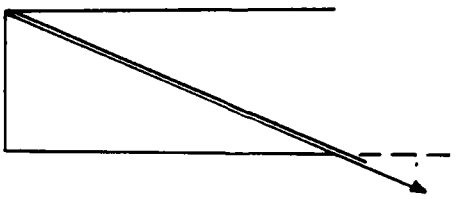

Fig. 2-10. Total Reflection

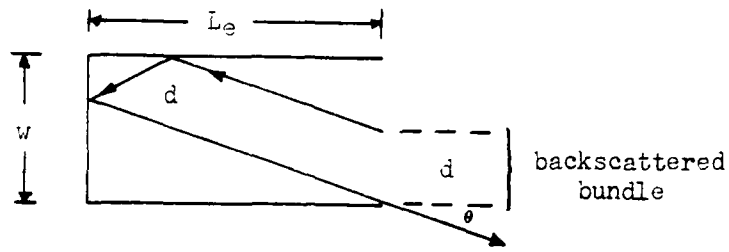

Fig. 2-9. Case 2 Cavity

percentage of the total power that is backscattered is given by

$$\% \text{ backscatter} = \frac{d}{w}$$

where

$$\tan \theta = \frac{w - d/2}{L_e}$$

therefore

$$d = 2(w - L_e \tan \theta)$$

and

$$\% \text{ backscatter} = 2\left[1 - \frac{L_e \tan \theta}{w}\right]$$

Once again there is a limiting case for a cavity of this length. When the effective cavity length exactly equals one-half of a cavity wavelength, all of the incident radar energy

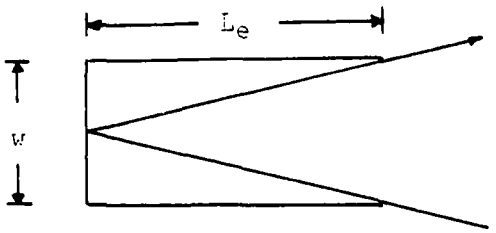

Fig. 2-8. Total Backscatter

and

$$\tan \theta = \frac{w/2}{\lambda/4} = \frac{w/2}{L_e}$$

or

$$\theta = \arctan \left[\frac{2w}{\lambda}\right] = \arctan \left[\frac{w}{2\ L_e}\right]$$

It should be noted that this total backscatter occurs only when L_e exactly equals $\lambda/4$. However, as L_e aproaches $\lambda/4$ the percentage of backscatter approaches 100%.

Case 2

This case occurs when the cavity's effective length is between one-quarter and one-half cavity wavelength. ($\lambda/4 < L_e < \lambda/2$). Fig. 2-9 shows a case 2 cavity with its boundary ray.

In this case, any incident ray entering below this boundary ray will be backscattered, and once again the

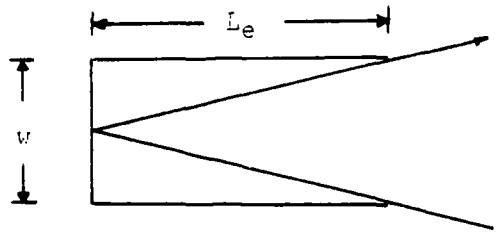

Fig. 2-8. Total Backscatter

and

$$\tan \theta = \frac{w/2}{\lambda/4} = \frac{w/2}{L_e}$$

or

$$\theta = \arctan \left[\frac{2w}{\lambda}\right] = \arctan \left[\frac{w}{2\ L_e}\right]$$

It should be noted that this total backscatter occurs only when L_e exactly equals $\lambda/4$. However, as L_e aproaches $\lambda/4$ the percentage of backscatter approaches 100%.

Case 2

This case occurs when the cavity's effective length is between one-quarter and one-half cavity wavelength. ($\lambda/4 < L_e < \lambda/2$). Fig. 2-9 shows a case 2 cavity with its boundary ray.

In this case, any incident ray entering below this boundary ray will be backscattered, and once again the

the entire power which is backscattered is

$$\% \text{ backscatter} = \frac{d}{w}$$

It can also be seen that

$$\tan \theta = \frac{d/2}{L_e}$$

therefore

$$d = 2 L_e \tan \theta$$

and

$$\% \text{ backscatter} = \frac{2 L_e \tan \theta}{w}$$

So, for the Case 1 cavity, the percentage of backscatter increases as θ increases.

When the effective cavity length exactly equals one-quarter of a wavelength, an interesting phenomenon occurs: all the radar energy is backscattered. This can be seen in Fig. 2-8 which shows the boundary ray for this case. The boundary ray lies exactly at the lower edge of the cavity opening, so all rays entering above it (all rays entering the cavity) are backscattered. This instance of total backscatter occurs when

$$L_e = \lambda/4$$

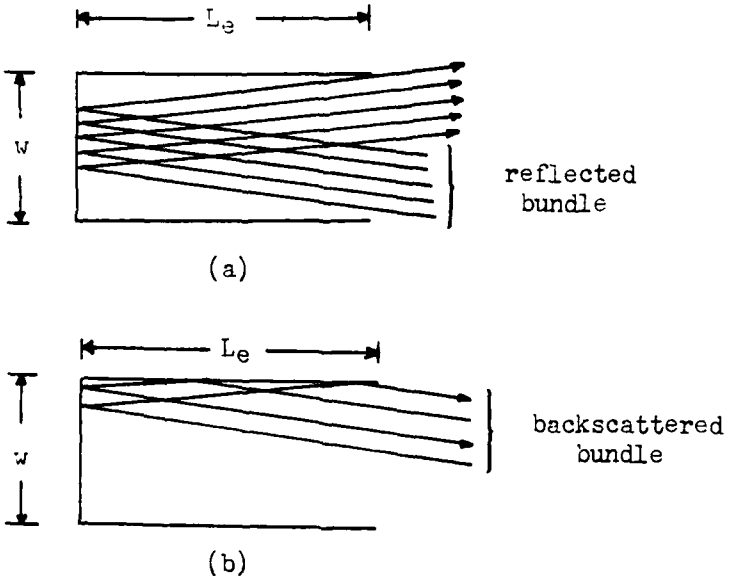

Fig. 2-6. Reflection and Backscatter

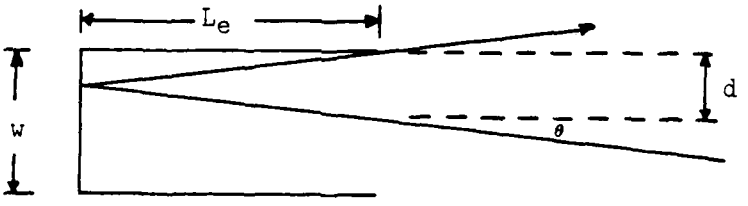

Fig. 2-7. Boundary Ray

Whereas the entire cavity has an opening of width w, that portion of the opening which admits backscattering rays has width d as shown in Fig. 2-7. Therefore, that portion of

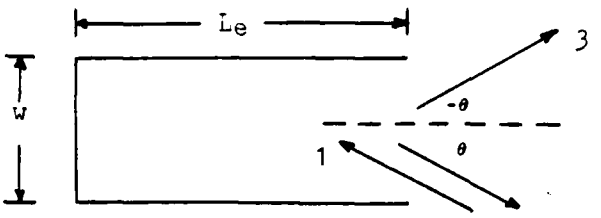

Fig. 2-5. General Case 1 Cavity

shows a general cavity with an effective length of less than one-quarter cavity wavelength. The incident radar energy enters the cavity at angle θ (arrow #1), but the exiting energy leaves at two different angles. Furthermore, the energy can only leave at these two angles. Part of the energy is scattered directly back toward the source at the angle θ (arrow #2), and the rest is reflected out of the cavity at an angle of -θ (arrow #3). Determining the power ratio between these two exit waves is the key to this analysis.

Figure 2-6(a) shows the ray bundle which is reflected (-θ). Fig. 2-6(b) shows the bundle which is backscattered (θ). Fig. 2-7 shows the boundary ray which divides these two ray bundles. Any rays entering the cavity below this boundary ray are reflected in the -θ direction. Rays entering above this boundary are backscattered in the θ direction.

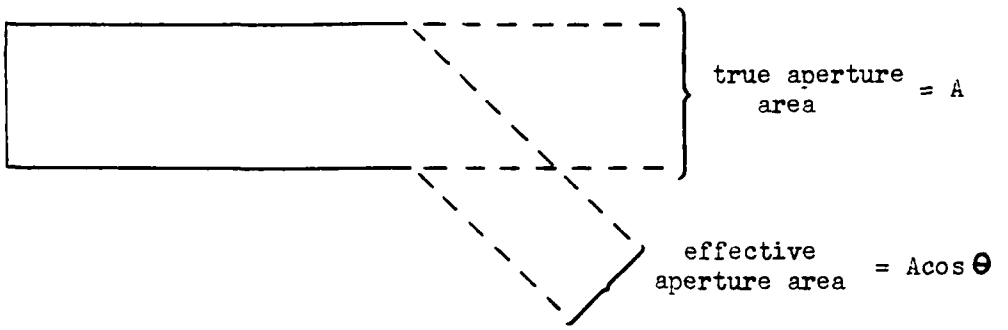

Fig. 2-4. Effective Aperture Area

Therefore, the first significant modulation of the cavity's peak RCS is the squared cosine of the incident angle.

The varying tradeoff between the two possible exit directions is a bit more complicated. However, the analysis is simplified considerably since the effective cavity length can not exceed one cavity wavelength. There are only four separate cases which must be analyzed, and each case deals with a separate one-quarter increment of a cavity wavelength as described below.

Case 1

This case occurs when the effective length (L_e) is under one-quarter of a cavity wavelength. ($0 < L_e < \lambda/4$) Fig. 2-5

The maximum radar cross section of the cavity occurs when $\theta = 0$ degrees. The entire back end of the cavity is in direct view at this aspect. It is well known that the radar cross section of a flat plate for high frequencies at normal incidence is:

$$\sigma(\theta = 0) = \frac{4\pi A^2}{\lambda_o^2}$$

where

A = area of the flat plate
λ_o = wavelength of the radar energy

This RCS is the maximum return from the cavity, and it occurs exactly at $\theta = 0$. As the incident angle is varied, this peak RCS is modulated by two separate phenomena. The first is caused by the changing effective aperture area, and the second is the varying tradeoff between the two possible exit directions (θ and $-\theta$).

As the incident angle θ increases, less radar energy is allowed to enter the cavity causing the RCS to decrease. This is shown in Fig. 2-4. The effective aperture area is proportional to the cosine of the incident angle.

As already noted, the radar cross section of a flat plate is proportional to its area squared, so:

$$\sigma = \frac{4\pi A_{eff}^2}{\lambda_o^2} = \frac{4\pi (A\cos\theta)^2}{\lambda_o^2} = \frac{4\pi A^2 \cos^2\theta}{\lambda_o^2}$$

therefore

$$\lambda = \frac{2w}{\tan \theta}$$

It is important to note that this cavity wavelength is a function of incident angle. Therefore, a new cavity wavelength must be calculated for each incident angle of interest. Then the maximum integer number of cavity wavelengths must be subtracted from the total length of the cavity to yield the effective cavity length. A further example of this process is displayed in Fig. 2-3. The cavity is over two wavelengths long as shown in Fig. 2-3(a), and once these two wavelengths are subtracted from the overall length, the effective cavity is shown in Fig. 2-3(b).

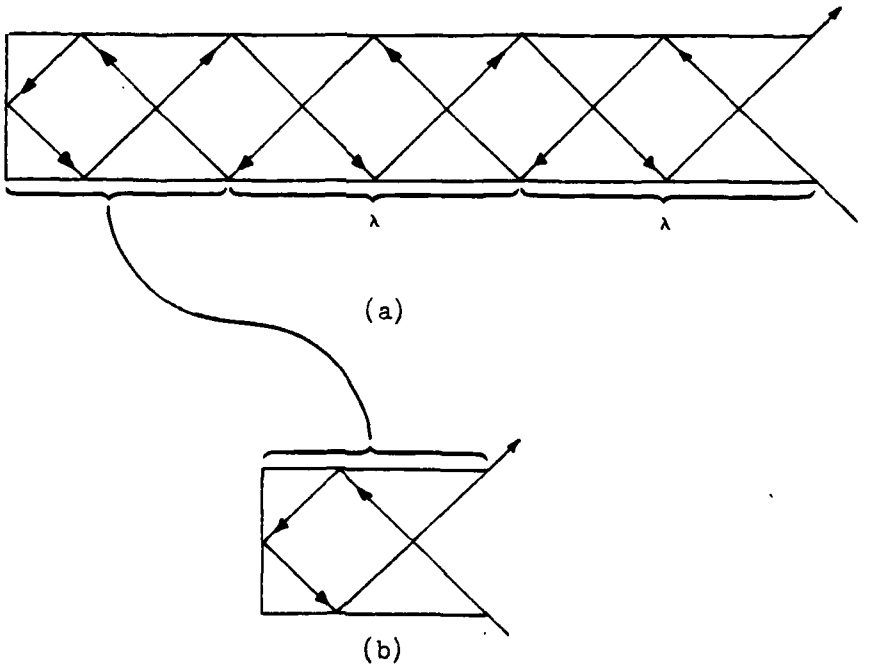

Fig. 2-3. Effective Cavity Length

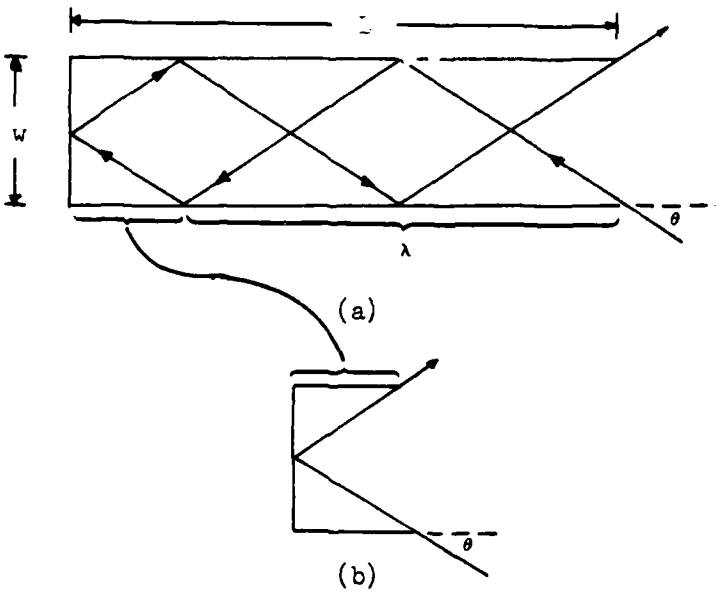

Fig. 2-2. Wavelength of a Two-Dimensional Cavity

scattering using this ray tracing analysis technique. Following one ray of the incident energy, it can be seen in both diagrams that entry and exit locations and directions are identical.

The distance of a complete cycle of bounces as shown in Fig. 2-2(a) is labeled as a "wavelength." This is not to be confused with the actual wavelength of the electromagnetic wave. The cavity wavelength is very important in the simplification of this analysis. It can be seen in Fig. 2-2(a) that

$$\tan \theta = \frac{W}{\lambda/2} = \frac{2w}{\lambda}$$

where

λ = cavity wavelength

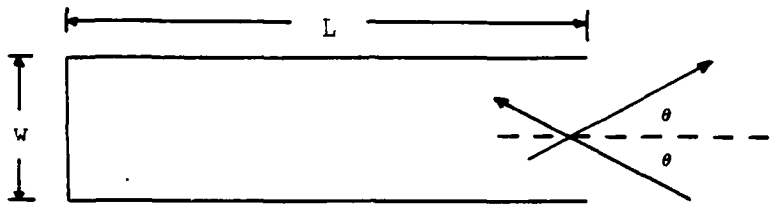

Fig. 2-1. General Two-Dimensional Cavity

algebraic equations to a two-dimensional plane. It is this limitation which make the analysis of the two-dimensional case considerably less complicated than the three-dimensional cavity.

It can be shown that as a first order approximation all energy entering the cavity from angle θ will exit at either that same angle θ or its mirror image (-θ). The ratio of the powers exiting in the two directions depends on the cavity's width and length as well as the incident angle θ.

But first, the structure of a two-dimensional cavity can be simplified somewhat. As shown in Fig. 2-2(a) for certain incident angles, the entering radar energy may "bounce" several times within the cavity before exiting. If this energy bounces off each side wall before it hits the cavity end, then the cavity can be analytically simplified. Fig. 2-2(b) shows an equivalent cavity which produces identical

The percentage of the total power that is backscattered is

$$\% \text{ backscatter} = \frac{d}{w}$$

where

$$\tan \theta = \frac{w - d/2}{L_e - \lambda/2}$$

or

$$d = 2(w - (L_e - \lambda/2)\tan \theta)$$

therefore

$$\% \text{ backscatter} = 2 \left[1 - \left[\frac{(L_e - \lambda/2)\tan \theta}{w}\right]\right]$$

When the effective cavity length exactly equals one cavity wavelength, all the incident energy will be reflected in the $-\theta$ direction. This total reflection is shown in Fig. 2-14. All rays entering the cavity above this boundary ray will be reflected.

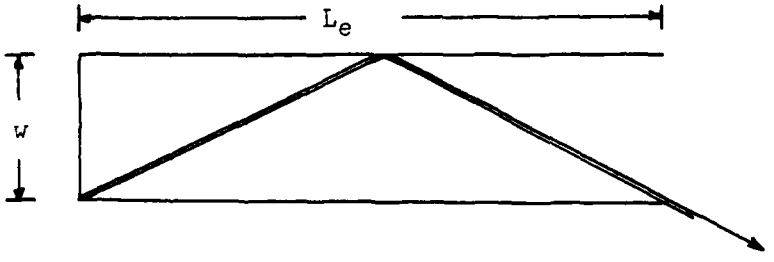

Fig. 2-14. Total Reflection

Summary

There are several steps necessary to conduct this ray tracing analysis.

Step 1: Calculate the peak RCS of the cavity using the following equation:

$$\sigma \text{ (peak)} = \frac{4\pi A^2}{\lambda_o^2}$$

Then, for each incident angle θ, the following steps must be performed:

Step 2: Multiply this peak RCS by $\cos^2\theta$ due to the varying effective aperture area. This modified RCS would be a final answer if all the energy was backscattered.

Step 3: Calculate the cavity wavelength according to the equation:

$$\lambda = \frac{2w}{\tan \theta}$$

Step 4: Subtract the maximum integer number of cavity wavelengths from the cavity's true length to yield the cavity's effective length.

$$L_e = L - (n \lambda)_{max}$$

Step 5: Depending on the effective length, calculate the percentage of backscatter according to the following equations.

L_e	% backscatter
$0 < L_e < \frac{\lambda}{4}$	$\frac{2 L_e \tan \theta}{w}$
$\frac{\lambda}{4} < L_e < \frac{\lambda}{2}$	$2\left[1 - \frac{L_e \tan \theta}{w}\right]$
$\frac{\lambda}{2} < L_e < \frac{3\lambda}{4}$	$2\left[\frac{(L_e - \lambda/2) \tan \theta}{w}\right]$
$\frac{3\lambda}{4} < L_e < \lambda$	$2\left[1 - \frac{(L_e - \lambda/2) \tan \theta)}{w}\right]$

Step 6: Finally, calculate the RCS as follows:

$$\sigma(\theta) = (\sigma_{peak})(\cos^2 \theta)(\% \text{ backscatter})$$

III. RCS Measurement of a Two-Dimensional Cavity

Introduction

It is the purpose of this thesis not only to develop the ray tracing theory as outlined in Chapter II but to formulate a computer program to accurately predict the RCS of a two dimensional cavity as well. However, unless the computer predictions can accurately compare to measured results, the theory and computer program are without value. Therefore, an important part of this project was the measurement of the RCS of an actual two dimensional cavity. This data was then used as a benchmark against which the computer predictions were compared.

Design of the Cavity

The primary difficulty associated with designing a two-dimensional cavity is that the surrounding structure's RCS must be low compared to the cavity's RCS for a wide range of incident angles. One such design, and the one which was eventually used, is shown in Fig. 3-1.

Embedding the cavity in a wedge-cylinder as shown provides several advantages. First, none of the supporting structure is normal to the radar except at large incident angles. And second, the cylinder behind the cavity prevents a large diffraction component from originating at the back

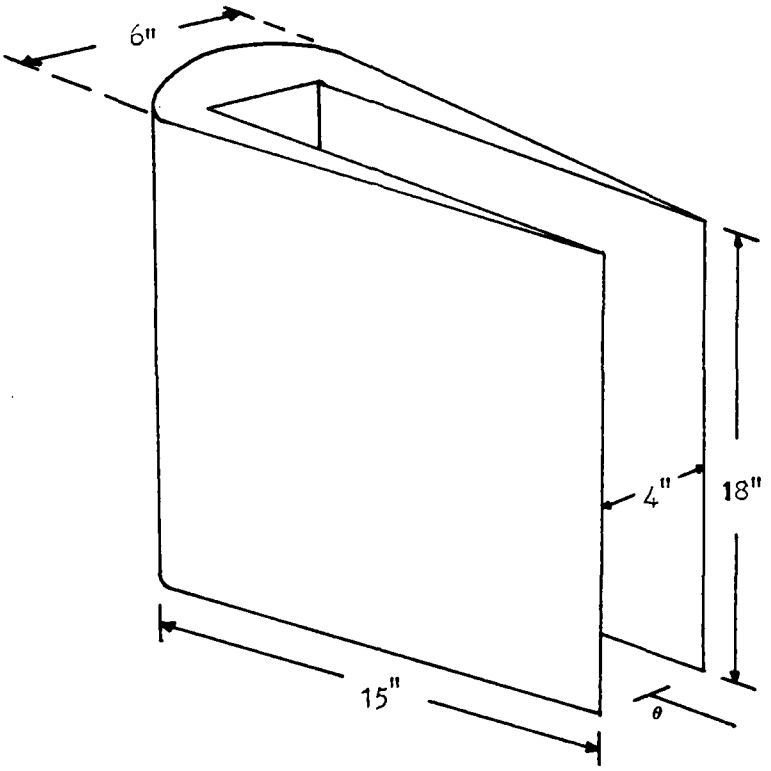

Fig. 3-1. Two Dimensional Test Cavity

edge of the side panels for horizontal polarization. The height of the cavity in the two-dimensional case should theoretically be infinite. However, for measurement purposes, a length of 18 inches was sufficient to fill the radar's main beam. Finally, the ratio between the cavity's width and depth was designed to approximate the ratio normally found in engine inlets.

Construction of the Cavity

The test cavity was fabricated at the AFIT model shop (Bldg. 597) by Mr. John Brohas. It was made out of aluminum because it was easiest to work with, and the entire cavity's

weight could not exceed 75 pounds due to limitations of the radar range's target pedestal. The finished aluminum test cavity weighed an unwieldy 66 pounds and was constructed from a solid cylinder and two flat plates which were planed down to form the wedge shaped cavity walls.

All the seams were sealed and smoothed to allow the propagation of traveling waves, and the two leading edges were sharpened to minimize the two edge returns for vertical polarization.

Test Facility

The measurement of the cavity's RCS was performed at the Passive Countermeasures Branch of the Air Force Wright Aeronautical Laboratory's Electronic Warfare Division (Bldg. 821) under the supervision of Dr. Robert Puskar and Mr. Ed Williams. The fully instrumented radar cross section range consists of an anechoic chamber, a rotating target pedestal, a computer control console, and several different platforms supporting radar transmitting and receiving equipment. The measurement procedure is started with a nulling out of the return of the range itself. These range returns are caused by the pedestal, walls, absorbing cones, and other structures. By adjusting the magnitude and phase of the signal (without a target) in a second receive channel which is added to the primary channel's signal, the range return can be nulled out. Next, the power level of the received signal must be calibrated. By placing a sphere of known RCS

(in this case -14 dBsm) on the pedestal and measuring its return, all future measurements can be compared to this benchmark. Then the test cavity is placed on the pedestal with the long dimension of the cavity's opening in the vertical direction. The cavity's RCS is then measured as it is rotated in the θ and $-\theta$ directions (θ is in the horizontal plane). The angles of interest lie between approximately -45 and 45 degrees because the returns from the side panels are too large beyond these aspects.

IV. Comparison of Results

Introduction

A computer program was written so that RCS values for the test cavity could be predicted for a wide range of incident angles. The computer code, along with complete documentation and details of its operation, is contained in Appendix A. The results from this program were compared to the actual test measurements so that a qualitative judgement of the usefulness of the ray tracing theory could be made.

Measurements

Measurements were made at a frequency 17.2 GHz for both horizontal and vertical polarizations because this was the highest frequency for which the test range had equipment. These results are shown in Fig. 4-1 and 4-2. There is obviously a significant difference between the two graphs for incident angles between -15 and +15 degrees. This could be caused by several factors. First, the cavity's two leading edges create more backscatter for vertical polarization because of currents which are set up along these edges. And second, horizontally polarized energy causes travelling waves to be set up on the cavity's sidewalls. This discrepancy highlights the fact that this test was not of a truly high frequency nature. Ideally, if the wavelength of the

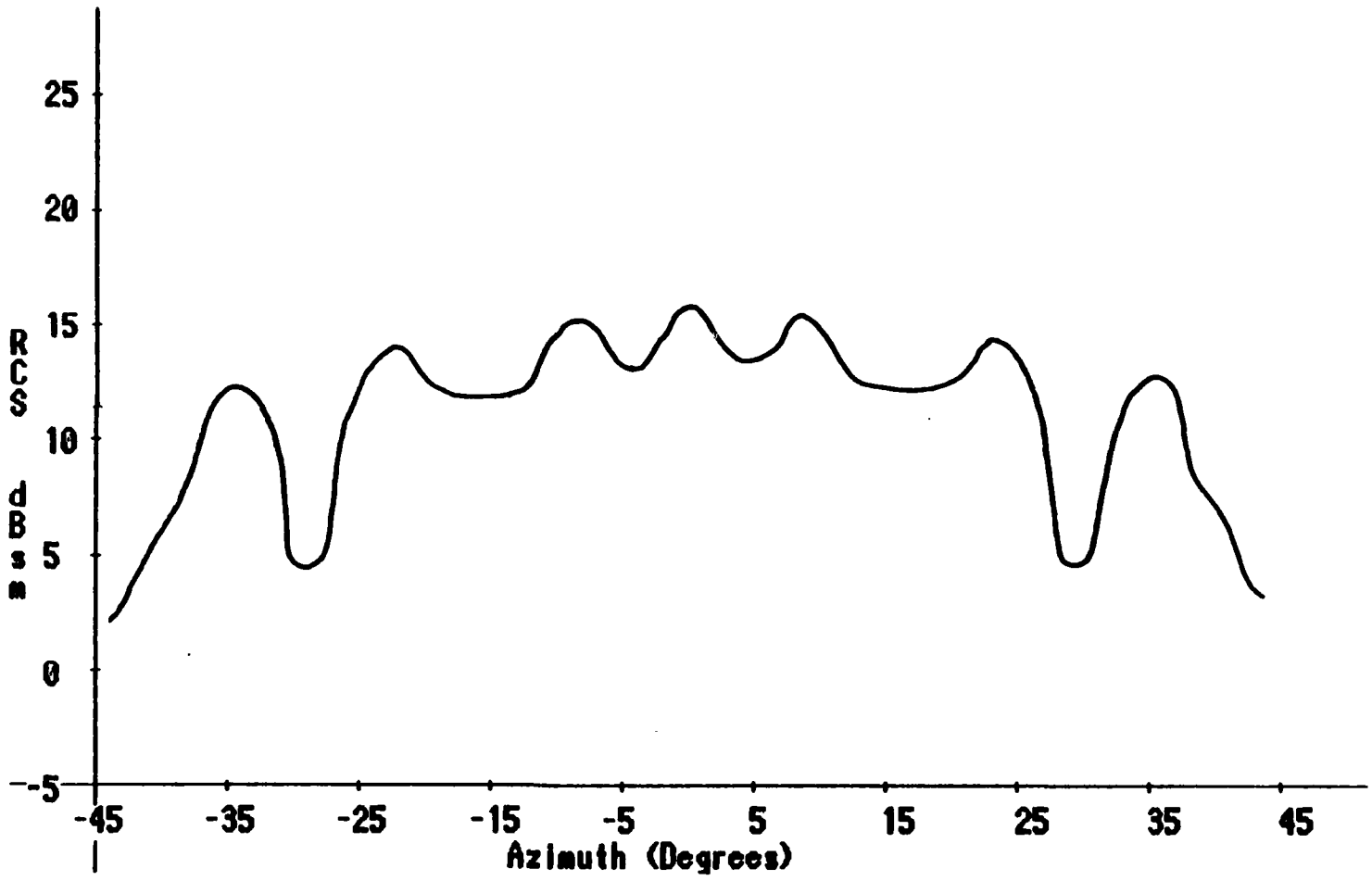

Fig 4-1. RCS Measurement at 17.2 GHz
(horizontal polarization)

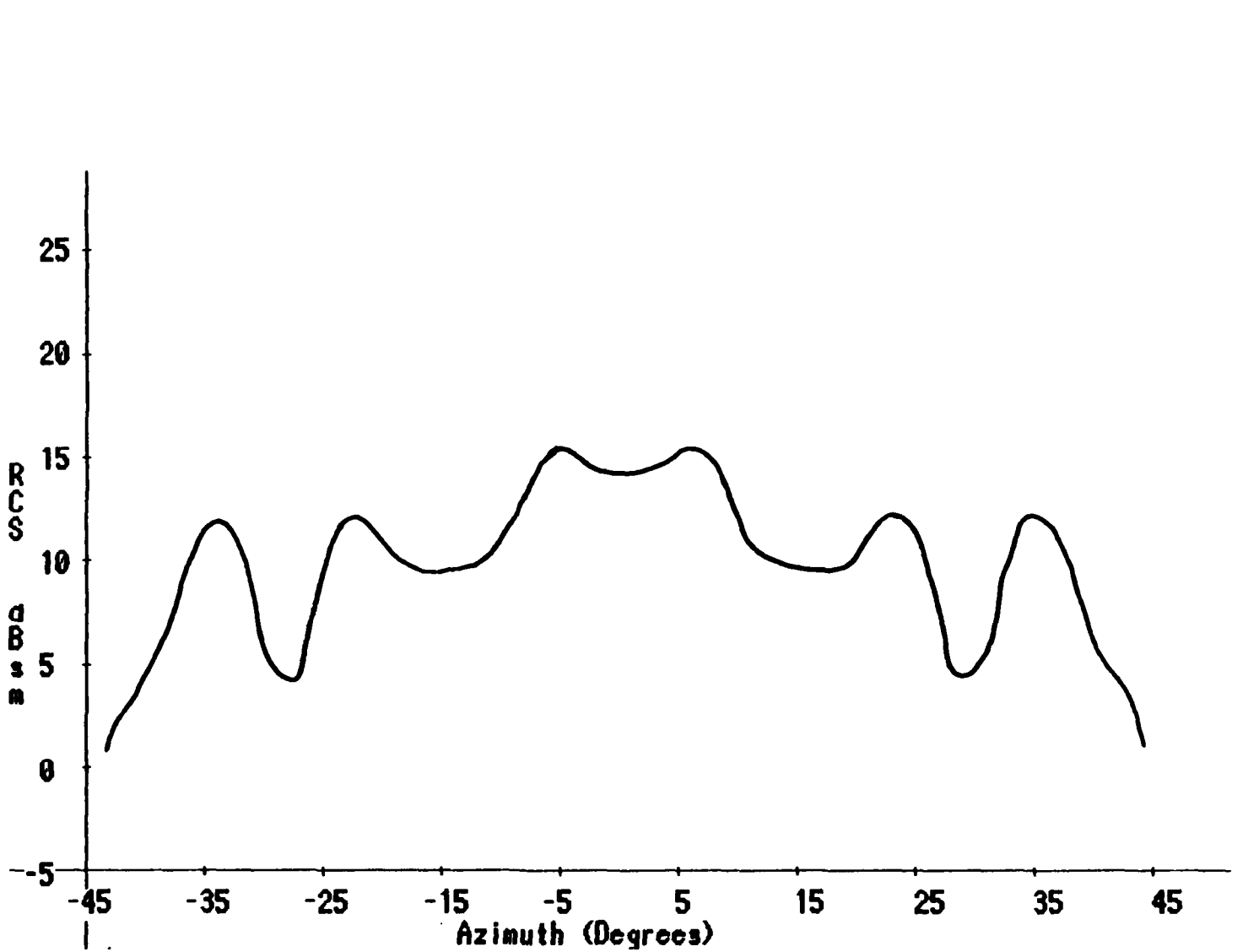

Fig 4-2. RCS Measurement at 17.2 GHz
(vertical polarization)

electromagnetic energy is small enough compared to the cavity's dimensions (particularly the width of the opening), then the measurements should be the same for both polarizations.

The measurements were plotted using a 5 degree averaging window. Thus, the RCS value for each incident angle is actually the average of RCS values for five degrees centered at that angle. This averaging technique smoothes out the curves so that RCS variations don't obscure the general trends.

It should be noted that for angles in excess of approximately 45 degrees off axis, the RCS of the cavity is dominated by the return from the large flat plate which serves as the outside wall of the wedge cylinder. Since only the return from the interior of the cavity is of interest for this thesis, comparisons of data beyond these angles is not made.

Computer Results

The results from the computer program are plotted in Fig. 4-3. Since the entire ray tracing approach assumes very high frequencies, these RCS values are independent of polarization.

RCS values were calculated for incident angles at one degree intervals. So that a fair comparison to the measured data could be made, a subroutine was devoted to generating a 5 degree averaging window.

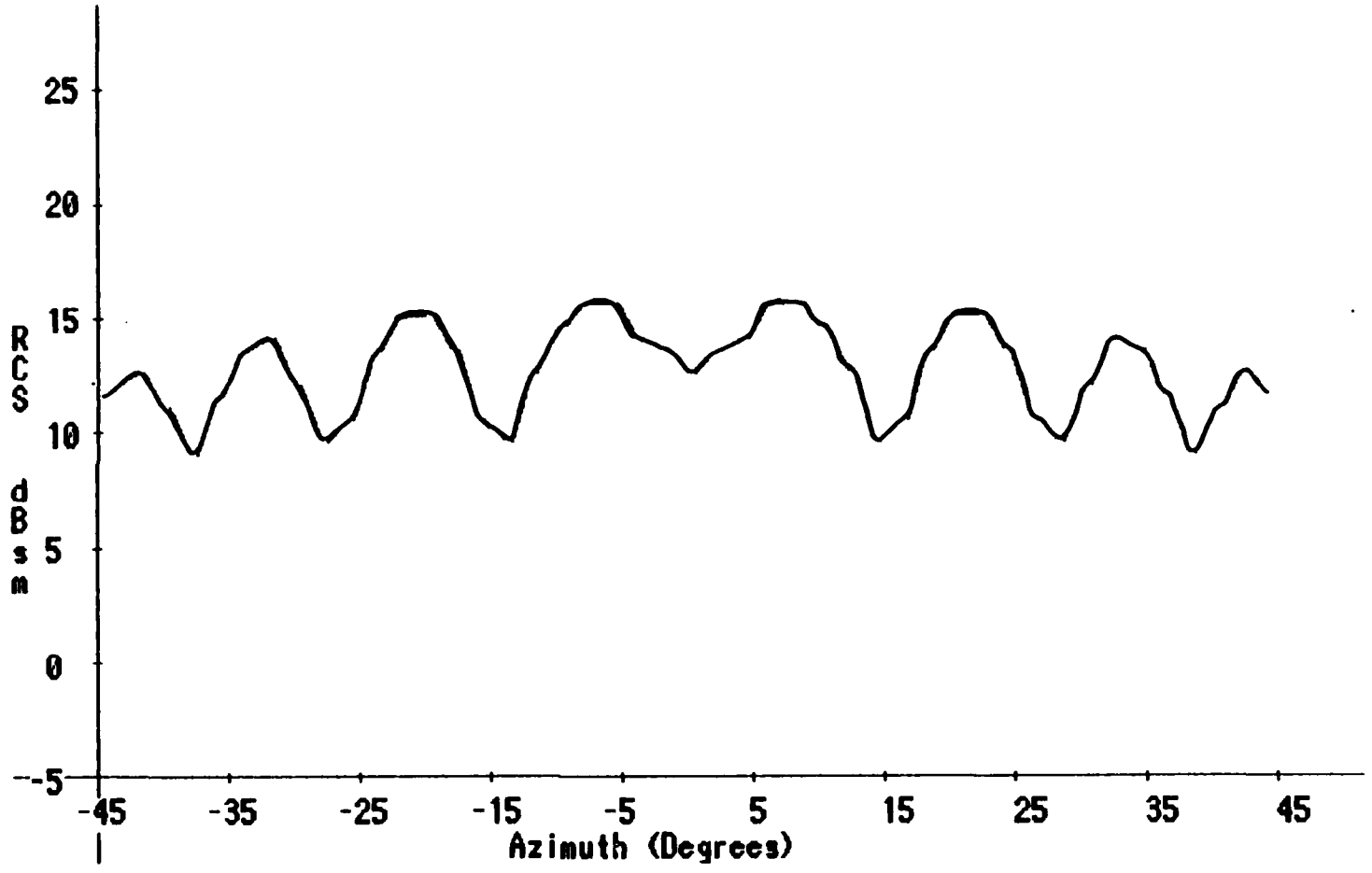

Fig. 4-3. RCS Computer Calculations

Also, calculations of predicted RCS values were only made for incident angles of no more than 45 degrees off-axis. The ray tracing approach neglects the RCS contribution of the outside of the wedge cylinder.

Comparison

Fig. 4-4 shows the computer data along with the measurements for horizontal polarization. It is clear that predictions for angles of less than ten degrees off axis are not accurate. Indeed, the shapes of the curves for these angles are not similar. However, beyond these angles, the ray tracing theory is more successful. It accurately predicts peaks at angles of approximately ± 22 degrees and ± 33 degrees. Nevertheless, although the trends are the same for these angles, the magnitude of the RCS peaks for the measured data falls off faster than the $\cos^2\theta$ decrease predicted by the ray tracing theory. This could be caused by the fact that as the incident angle increases, the effective width of the cavity decreases causing the test to be less and less of a high frequency case. This causes the theory to be decreasingly valid as the incident angle increases.

Fig. 4-5 shows the same computer data compared to the measurements for vertical polarization. Here the agreement is much more striking. The overall shapes of the two curves are very similar with the computer accurately predicting the angles at which RCS peaks occur. The agreement is also quite

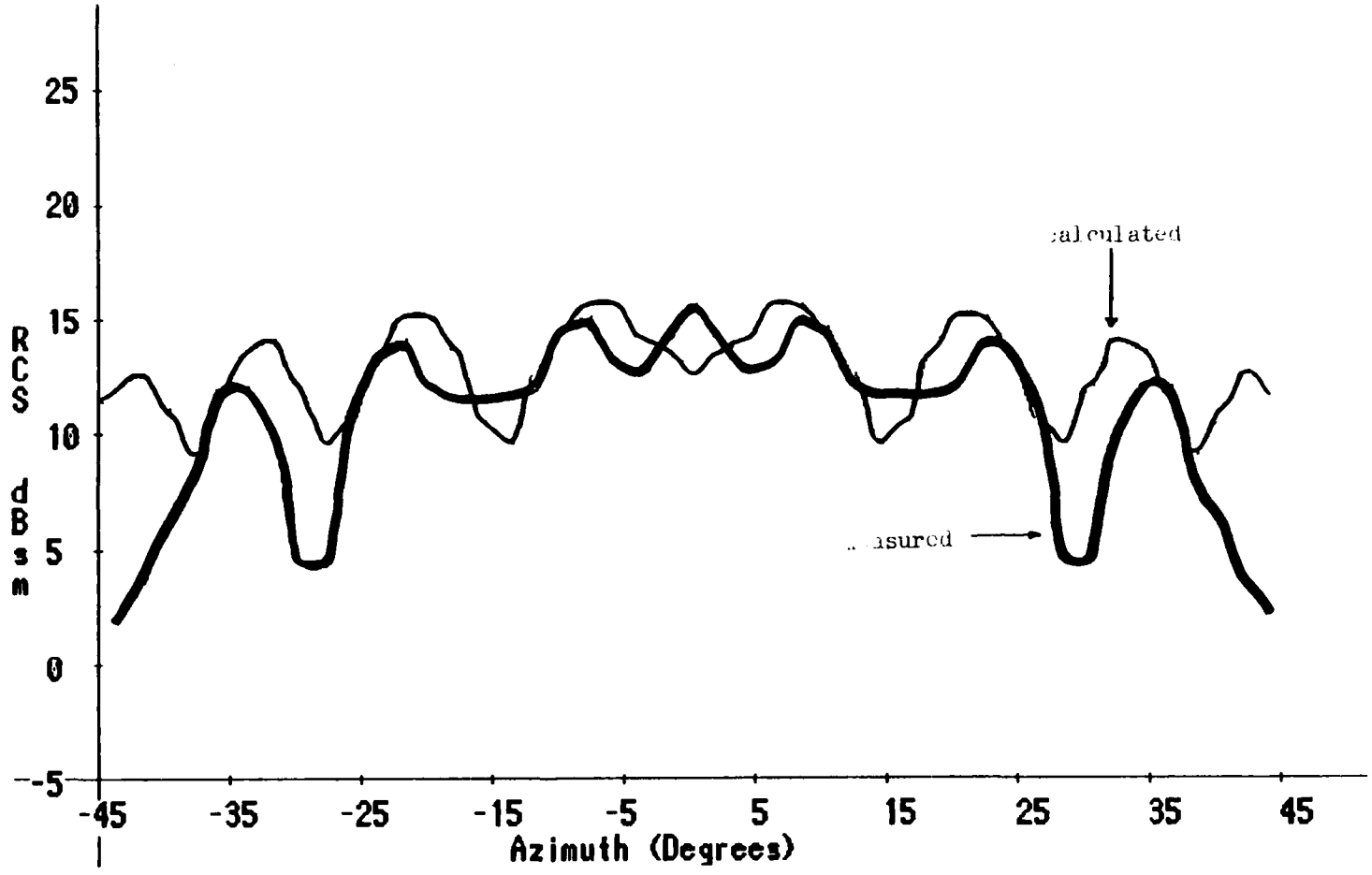

Fig. 4-4. RCS Measurements and Computer Calculations (horizontal polarization)

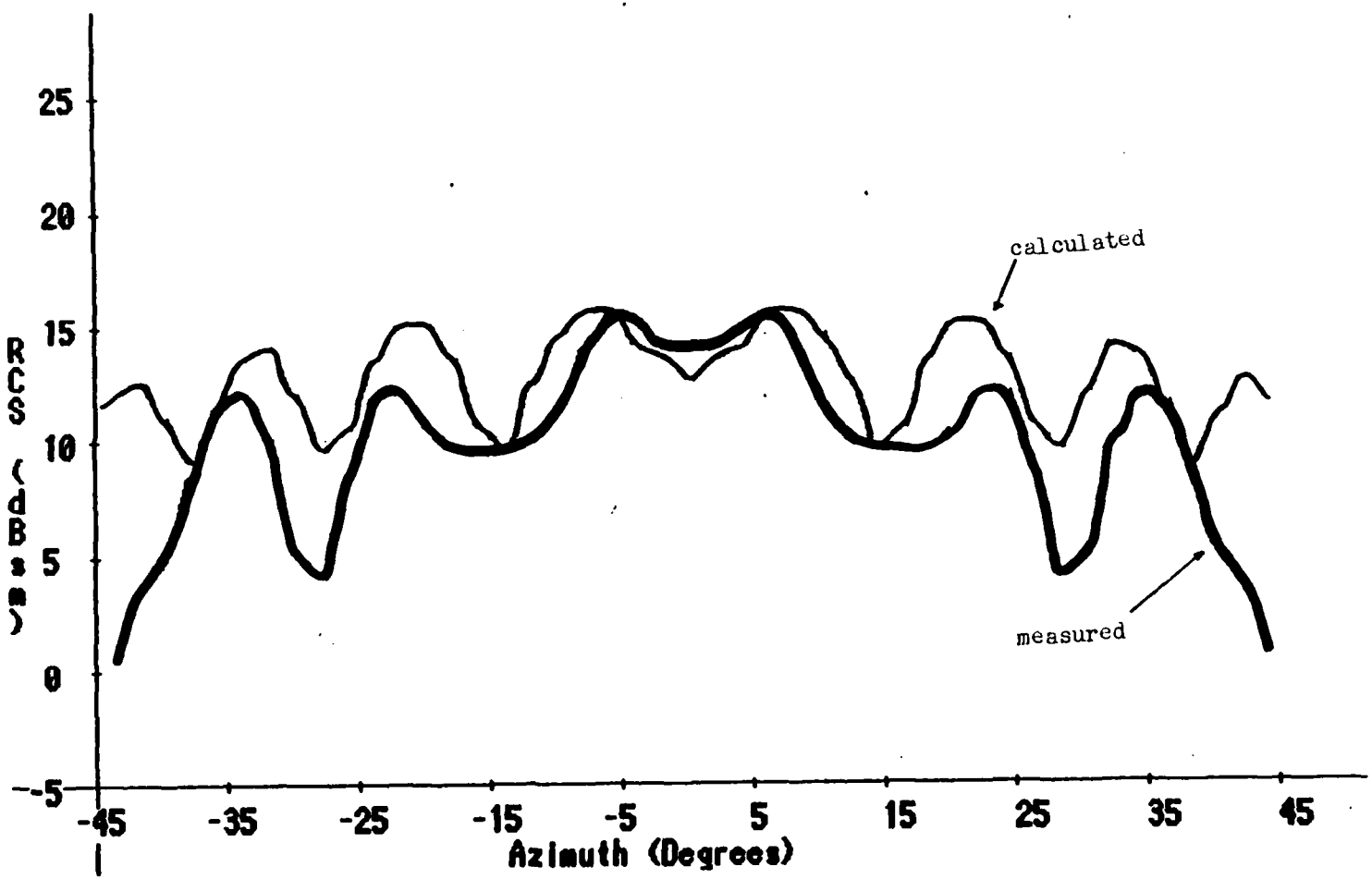

Fig. 4-5. RCS Measurements and Computer Calculations (vertical polarization)

good for small angles in contrast to the horizontal polarization case. Once again, however, the computer code predictions do not fall off as fast as the measured data. Nevertheless, these results are very encouraging. Evidently the horizontally polarized wave is more sensitive to the ratio between wavelength and cavity width. In other words, since the theory agrees more closely with the vertical polarization case, perhaps the measured results for vertical polarization more closely approximate the truly high frequency case.

V. Conclusions and Recommendations

Conclusions

Overall, the comparison between the computer calculations and the measurements was encouraging enough to show that the ray tracing approach shows some promise for limited application. From the outset it was obvious that this approach is limited to high frequencies, but this does not mean the theory is without application. Because it is straightforward enough to be implemented by a short and streamlined computer program, this technique can provide considerable savings of computer execution time and storage requirements when compared to some of the more widely applicable methods described in Chapter I.

The discrepancies between the measured and calculated RCS values for vertical polarization as outlined in Chapter IV are probably caused by one of two phenomena. First, as mentioned previously, it could be caused by the decreasing aperture width forcing the cavity to approach the low frequency case. If this is indeed the cause of the less than perfect data agreement, then it demonstrates the lower limits of the model's applicability. And, the computer code in its present form should become increasingly accurate for higher frequencies. Another possibility exists, however. The progressive gap between the data could be caused by a failure

to account for diffraction of the radar wave both as it enters and exits the cavity. If this is the problem, then the discrepancy will persist for all frequencies thus representing a flaw in the theory. Nevertheless, a diffraction coefficient subroutine as described by Kouyoumjian and Pathak (3) could be easily included in the computer program without serious execution time penalties.

Recommendations

Since the ray tracing approach to cavity scattering shows promise, it may merit some additional work in the future. If further work is deemed appropriate, the following items should be accomplished. First, future tests should either use higher frequencies or larger cavity dimensions to ensure that low frequency phenomena do not distort the data. Since the theory is a high frequency method, any tests should use frequencies which are "high enough." If this does not solve the problem of the less than desirable data agreement for large incident angles, then a diffraction coefficient subroutine should be included to find out if this indeed is the cause of the problem. Furthermore, different models should be tested to make sure the theory works for cavities of different widths and depths. This will serve to validate this approach for a general cavity rather than for just one specific shape. Finally, and most importantly, the ray tracing theory should be extended from two into three dimensions. Whereas two-dimensional cavities are almost non-

existant in the real world, three-dimensional cavities can be found in prodigious numbers. Therefore, the ultimate application of this technique depends upon its extension to handle three-dimensional cavities. While this task is not trivial, it is certainly more painstaking than complicated.

Bibliography

1. Cooper, Lt. Thomas G. A Finite Element Computation of the Electromagnetic Fields Within an Engine Inlet Model. MS Thesis, School of Engineering, Air Force Institute of Technology (AU), Wright-Patterson AFB OH, December 1982.

2. Johnson, Thomas W. and D. L. Moffatt. Electromagnetic Scattering by Open Circular Waveguides. PhD dissertation. Ohio State University, December 1980.

3. Kouyoumjian, R. G. and P. H. Pathak. "A Uniform Geometrical Theory of Diffraction for an Edge in a Perfectly Conducting Surface," Proceedings of the IEEE, 62: 1448-1461 (1974).

4. Moll, John W. and Rolf G. Seecamp. "Calculation of Radar Reflecting Properties of Jet Engine Intakes Using a Waveguide Model," IEEE Transactions on Aerospace and Electronic Systems, AES-6(5): 675-683 (September 1970).

```
100 REM      THIS PROGRAM WAS WRITTEN BY R.SCOTT DERING
110 REM      IN AUGUST 1984.  IT RUNS ON A TOSHIBA T-100
120 REM      PERSONAL COMPUTER.  IT CALCULATES THE RCS
130 REM      OF THE TWO-DIMENSIONAL CAVITY DESCRIBED IN
140 REM      CHAPTER III USING THE RAY TRACING METHOD AS
150 REM      OUTLINED IN CHAPTER II.
160 REM
170 REM
180 REM
190 CLEAR
200 DEFSNG A-M,O-Z
210 DIM MAG(50),ARRAY(100),RCS(100)
220 REM
230 REM     FIRST, COMPUTE THE PEAK RCS OF THE CAVITY
240 REM     WHICH IS ACTUALLY THE RCS OF THE SQUARE FLAT
250 REM     PLATE AT THE END OF THE CAVITY
260 REM
270 REM LAMBDA IS FREE SPACE WAVELENGTH
280 REM
290 REM AREA IS THE AREA OF THE CAVITY END
300 REM
310 LAMBDA=.02
320 AREA=.044
330 W=.1
340 LENGTH=.385
350 PEAK=4*3.14159*(AREA^2)/(LAMBDA^2)
360 REM
370 REM  NOW THE PEAK RCS MUST BE SCALED ACORDING TO
380 REM  THE THEORY OUTLINED IN CHAPTER II.
390 REM
400 FOR N=1 TO 50 STEP 1
410 REM
420 REM FIND THE "CAVITY WAVELENGTH"
430 REM
440 THETA =N/57.3
450 WAVEL=2*W/(TAN(THETA))
460 L=LENGTH
470 REM
480 REM DECIDE WHICH CASE APPLIES (1,2,3, OR 4)
490 REM
500 IF L =.25*WAVEL GOTO 960
510 IF L =.5*WAVEL GOTO 990
520 IF L =.75*WAVEL GOTO 1020
530 IF L =WAVEL GOTO 1060
540 L=L-WAVEL
550 GOTO 500
560 REM
```

```
570 REM SCALE THE RCS BY THE COSINE SQUARED FACTOR
580 REM
590 PERCENT=PERCENT*(COS(THETA))^2
600 REM
610 REM MAG(N) IS THE MAGNITUDE OF THE RCS FOR ANGLE N
620 REM
630 MAG(N)=PEAK*PERCENT
640 NEXT
650 MAG(0)=PEAK
660 REM
670 REM ASSIGN RCS VALUES TO NEGATIVE ANGLES AS WELL
680 REM
690 FOR N=0 TO 50 STEP 1
700 ARRAY(N+50)=MAG(N)
710 ARRAY(50-N)=MAG(N)
720 NEXT
730 REM
740 REM
750 LPRINT "ANGLE (DEG.)", "RCS"
760 REM
770 FOR N=2 TO 98 STEP 1
780 LPRINT "--------------------"
790 REM
800 REM
810 REM  AVG5 IS THE AVERAGE RCS OVER THE 5 DEGREE WINDOW
820 REM
830 AVG5=(ARRAY(N-2)+ARRAY(N-1)+ARRAY(N)+ARRAY(N+1)+ARRAY(N+2))/5
840 REM
850 REM  RCS(N) IS THE AVERAGE RCS FOR ANGLE N IN DECIBELS
860 REM
870 RCS(N)=10*LOG(AVG5)*.43429
880 LPRINT N-50,RCS(N)
890 NEXT
900 END
910 REM
920 REM  THE FOLLOWING SECTIONS COMPUTE THE SCALING
930 REM  FACTORS FOR EACH OF THE FOUR CASES ACCORDING
940 REM  TO THE EQUATIONS LISTED ON PAGE 36.
950 REM
960 REM  CASE 1
970 PERCENT =2*L*(TAN(THETA))/W
980 GOTO 590
990 REM  CASE 2
1000 PERCENT =2*(1-L*TAN(THETA)/W)
1010 GOTO 590
1020 REM CASE 3
1030 LPRIME =L-.5*WAVEL
1040 PERCENT=2*LPRIME*TAN(THETA)/W
1050 GOTO 590
1060 REM CASE 4
1070 LPRIME=L-.5*WAVEL
1080 PERCENT=2*(1-LPRIME*TAN(THETA)/W)
1090 GOTO 590
```

Vita

Lieutenant Robert Scott Dering was born on 18 June 1959 in Springfield, Massachusetts. He graduated from Island Trees High School in Levittown, N.Y. in 1977, and he was a distinguished graduate from the Air Force Academy in 1981 receiving a Bachelor of Science in Electrical Engineering. He then served as an Electronic Warfare System Analyst at the Air Force Electronic Warfare Center, Electronic Security Command, in San Antonio, Texas until entering the School of Engineering, Air Force Institute of Technology, in June 1983.

Permanent Address: 35 Coppersmith Rd.
Levittown, N.Y. 11756

Unclassified

SECURITY CLASSIFICATION OF THIS PAGE

REPORT DOCUMENTATION PAGE

1a. REPORT SECURITY CLASSIFICATION Unclassified	1b. RESTRICTIVE MARKINGS
2a. SECURITY CLASSIFICATION AUTHORITY	3. DISTRIBUTION/AVAILABILITY OF REPORT Approved for public release; distribution unlimited
2b. DECLASSIFICATION/DOWNGRADING SCHEDULE	
4. PERFORMING ORGANIZATION REPORT NUMBER(S)	5. MONITORING ORGANIZATION REPORT NUMBER(S)
6a. NAME OF PERFORMING ORGANIZATION School of Engineering Air Force Institute of Tech. — 6b. OFFICE SYMBOL (If applicable) AFIT/ENG	7a. NAME OF MONITORING ORGANIZATION
6c. ADDRESS (City, State and ZIP Code)	7b. ADDRESS (City, State and ZIP Code)
8a. NAME OF FUNDING/SPONSORING ORGANIZATION — 8b. OFFICE SYMBOL (If applicable)	9. PROCUREMENT INSTRUMENT IDENTIFICATION NUMBER
8c. ADDRESS (City, State and ZIP Code)	10. SOURCE OF FUNDING NOS. PROGRAM ELEMENT NO. / PROJECT NO. / TASK NO. / WORK UNIT NO.
11. TITLE (Include Security Classification) See Box 19	

12. PERSONAL AUTHOR(S)
R. Scott Dering, 1Lt., USAF

13a. TYPE OF REPORT	13b. TIME COVERED	14. DATE OF REPORT (Yr., Mo., Day)	15. PAGE COUNT
MS Thesis	FROM ____ TO ____	1984 December	49

16. SUPPLEMENTARY NOTATION

17. COSATI CODES			18. SUBJECT TERMS (Continue on reverse if necessary and identify by block number)
FIELD	GROUP	SUB. GR.	Radar Reflections,
20	14		Aircraft Engine Ducts,
			Ray Tracing.

19. ABSTRACT (Continue on reverse if necessary and identify by block number)

Title: High Frequency Estimation of Two-Dimensional Cavity Scattering

Thesis Chairman: Andrew J. Terzuoli
Assistant Professor of Electrical Engineering

20. DISTRIBUTION/AVAILABILITY OF ABSTRACT UNCLASSIFIED/UNLIMITED ☒ SAME AS RPT. ☐ DTIC USERS ☐	21. ABSTRACT SECURITY CLASSIFICATION Unclassified
22a. NAME OF RESPONSIBLE INDIVIDUAL Andrew J. Terzuoli	22b. TELEPHONE NUMBER (Include Area Code) (513) 255-3576 — 22c. OFFICE SYMBOL AFIT/ENG

DD FORM 1473, 83 APR — EDITION OF 1 JAN 73 IS OBSOLETE.

SECURITY CLASSIFICATION OF THIS PAGE

Abstract:

A simple ray tracing approximation for the high frequency scattering from a two-dimensional cavity is developed. Whereas many other cavity scattering algorithms are very time consuming, this method is very swift.

The analytical development of the ray tracing approach is performed in great detail, and it is shown how the radar cross section (RCS) depends on the cavity's length and width along with the radar wave's angle of incidence. This explains why the cavity's RCS oscillates as a function of incident angle. The RCS of a two-dimensional cavity was measured experimentally, and these results were compared to computer calculations based on the high frequency ray tracing theory. The comparison was favorable in the sense that angular RCS minima and maxima were exactly predicted even though accuracy of the RCS magnitude decreased for incident angles far off-axis. Overall, once this method is extended to three dimensions, the technique shows promise as a fast first approximation of high frequency cavity scattering.

END

FILMED

5-85

DTIC